Karl F. Warnick

Microwave Connector De-Embedding and Antenna Characterization

Sagar K. Dhar, Mohammad S. Sharawi, and Fadhel M. Ghannouchi

This article describes a systematic procedure for microwave connector de-embedding in a single-port antenna system. Coaxial connectors are a much-used medium to probe the electrical properties of radio-frequency (RF) components. However, connectors impact the magnitude and phase response of the device under test (DUT). Thus, it is essential to de-embed the connector properties to access the actual characteristics of the DUT. Various de-embedding techniques reported in the literature considered the DUT as a two-port device.

A detailed and accurate procedure for connector de-embedding in a single-port antenna system in the context of active antenna design is demonstrated in this article. For this purpose, a continuous two-port antenna model is derived, and the results of connector de-embedding are presented with active antenna examples. Such a de-embedding procedure is an essential step in active antenna system design. The proper connector de-embedding step increases the accuracy and overall performance of the active antenna system.

Digital Object Identifier 10.1109/MAP.2018.2818002
Date of publication: 4 June 2018

EDITOR'S NOTE

In this issue's "Education Corner" column, authors Sagar K. Dhar, Mohammad S. Sharawi, and Fadhel M. Ghannouchi describe a detailed procedure of de-embedding microwave connectors from single-port antenna system measurement data and look into the traditional methods and ways to characterize microwave connectors and provide a systematic procedure for de-embedding connector effects from single-port antenna systems. This article provides several examples of the method's usefulness in the context of an active antenna system design.

ANTENNAS AS PART OF RF SYSTEMS

Traditionally, antennas and RF front-end electronic systems are designed separately and cascaded assuming 50-Ω port impedance. But an antenna can also be designed as an integral part of RF systems serving more than simply a radiating element. For example, antenna integrated oscillators are reported in [1]–[3], where the antenna provides a feedback path and improves the phase noise characteristics (by the high selectivity nature of microstrip antennas) with a simple single-ended oscillating architecture. High-efficiency power amplifiers are reported in [4] and [5] where harmonic tuning is achieved by a dielectric resonator antenna and a microstrip antenna, respectively. On the other hand, interesting antenna characteristics are also achieved from integrated active antenna systems, such as antenna miniaturization [1], [6], bandwidth enhancement [7], [8], and improved radiation performance [9].

One of the initial steps in active antenna system implementation is to characterize the antenna for which measurement results are preferred to avoid discrepancy in the subsequent steps. Generally, coaxial connectors are used to probe the characteristics of the microwave components and circuits. It is important to remember that connectors affect both the magnitude and phase responses of the circuit unless their properties are de-embedded.

MICROWAVE CONNECTOR CHARACTERIZATION

The first step in antenna characterization from measured data is the

 1045-9243/18©2018IEEE

connector characterization and de-embedding their effects. Generally, microwave connectors are modeled and characterized as two-port networks by lumped/distributed equivalent circuits, electromagnetic computer-aided design simulations, or analytical techniques. In these methods, the two-port parameters are calculated from the measured or simulation data. Microwave connector characterization by electromagnetic simulator and circuit approximations are presented in [10] and [11], respectively. On the other hand, a measurement-based analytical procedure for connector characterization is presented in [12], which is followed in this article because of its fewer assumptions and measurement-based calculations. However, the assumption of the ideal transmission lines (T-lines) made in [12] is avoided for better accuracy.

First, connectors are considered as reciprocal two-port devices and can be represented as a T-network as shown in Figure 1, where Z_{ij} is the connector impedance parameter and can be described as

$$Z_{ij} = \frac{V_i}{I_j}(I_k = 0, k \neq j). \quad (1)$$

Then, the 50-Ω microstrip T-line with the connectors is represented as the network shown in Figure 2(a), assuming the T-line to be symmetric and reciprocal where W, X, and Y are the T-network components of the connectors and M and N are the T-network components of the transmission line as defined in (2). The network can be again represented as an equivalent T-network as shown in Figure 2(b), where Z_{ij} represents the impedance parameters of the T-line with connectors. Applying (1) on the network

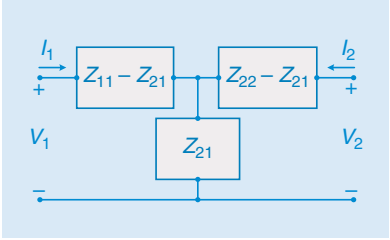

FIGURE 1. The equivalent circuit model of a connector assuming a reciprocal device.

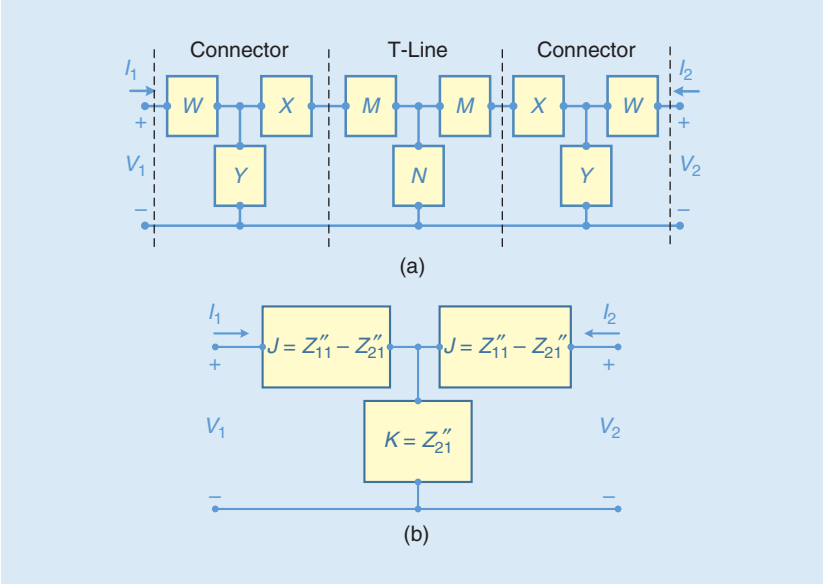

FIGURE 2. The equivalent circuit model of a transmission line (T-line) with the connectors.

shown in Figure 2(a) and comparing it with Figure 2(b) reveals two relationships between W, X, Y and J, K, M, N. However, another relationship is necessary to find a unique solution for W, X, and Y. Two T-lines with different lengths, as shown in Figure 3, can be used, and the unique relationships between W, X, Y and J, K, M, N can be deduced as expressed in (3)–(10) [12], where subscripted notations with 1 and 2 indicate the parameters for T-lines 1 and 2, respectively. Among possible different solutions of W, X, and Y, the correct ones are determined by enforcing power conservation rules as shown in

$$\begin{aligned} W &= Z_{11} - Z_{21} \\ &\quad (\text{connector } Z - \text{parameters}) \\ X &= Z_{22} - Z_{21} \\ &\quad (\text{connector } Z - \text{parameters}) \\ Y &= Z_{21} \ (\text{connector } Z - \text{parameters}) \\ M &= Z'_{11} - Z'_{21} \\ &\quad (T - \text{Line } Z - \text{parameters}) \\ N &= Z'_{21} \ (T - \text{Line } Z - \text{parameters}), \end{aligned} \quad (2)$$

$$Y = \pm\sqrt{\frac{-F}{2E} \pm \sqrt{\left(\frac{F}{2E}\right)^2 + \frac{H}{E}}}, \quad (3)$$

$$X = -(N_1 + M_1 + Y) \pm \sqrt{N_1^2 + \frac{N_1 Y^2}{K_1}}, \quad (4)$$

$$W = J_1 - \frac{Y(X + M_1)}{X + M_1 + Y}, \quad (5)$$

$$P = (N_2 - N_1) + (M_2 - M_1), \quad (6)$$

$$Q = (P^2 - N_1^2 - N_2^2)/2, \quad (7)$$

$$R = \frac{N_1}{2K_1} + \frac{N_2}{2K_2}, \quad (8)$$

$$F = S(N_1K_1 + N_2K_2) + 2QR, \quad (9)$$

and

$$H = Q^2 - (N_1N_2)^2. \quad (10)$$

By knowing the measured Z-parameters of the two T-lines with the connectors and equating to the Z-parameters of the network as shown in Figure 2, the S-parameters of the subminiaturized version A (SMA) connectors are calculated following the procedure in [12] and shown in Figures 4 and 5. However, we assume the parameters M and N to be ideal, T-lines are modeled, and their parameters M and N are

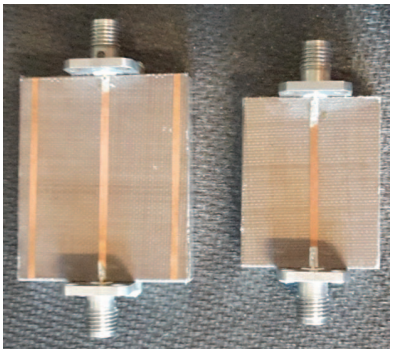

FIGURE 3. The T-line test prototypes.

calculated using the CST software. It can be seen that the connectors show linear phase characteristics over the frequency range while the transmission loss increases. This is because of the deviation of the impedance characteristics of the SMA connectors from the 50-Ω ideal value, which can also be observed by the higher reflection coefficients as the frequency increases. That is, these results emphasize that the connector effects should not be ignored.

DE-EMBEDDING AND ANTENNA CHARACTERIZATION

To access the actual antenna parameters from the measurement data, it is essential to de-embed the connector properties. De-embedding fringing capacitance and port discontinuities [13], [14], integrated circuit pads and parasitics [15]–[17], and printed circuit board interconnects [18] are discussed in the literature. However, all of these works addressed the de-embedding problem from the two-port network perspective. Although de-embedding the connectors' effect from an antenna array is presented in [19], this approach again is not suitable for a single-port antenna system. This article describes a generic de-embedding procedure of microwave connectors from a single-port antenna system.

In this regard, one easier and quicker way to approach this issue is with the port extension (PE) feature of a vector network analyzer (VNA) [20]. With this feature, the equivalent electrical delay of the connectors is calculated by open and/or short calibration steps, and the reference plane is shifted by the same amount, compensating for the effect of the measurement fixtures (in this case, the connectors). To assess this feature, a patch antenna is measured, and the results are shown in Figure 6. It can be seen that the PE feature actually compensates for the phase delay (the rotational shift on the Smith chart) introduced by the connectors. In this procedure, the VNA assumes the connector impedance to be 50-Ω, but the connectors are not lossless and not always 50-Ω, which can be observed from the connector S-parameters presented in Figures 4 and 5. Thus, a more accurate process of connector de-embedding is necessary, especially in the context of an active integrated antenna system design.

This article describes a generic de-embedding procedure of microwave connectors from a single-port antenna system.

A generic approach to de-embedding connector/test fixture effects is to embed the inverse ABCD matrix of the connector/fixture in the network [13]. For example, knowing the connector ABCD matrix, the measured T-line parameters of the network shown in Figure 2 can be determined by embedding the inverse connector ABCD matrices as expressed in (11), where $A_C B_C C_C D_C$ and $A_L B_L C_L D_L$ are the connector and T-line ABCD parameters, respectively. The two-port ABCD parameters are required in this approach, which cannot be directly determined from the single-port antenna measurement data. One approach adopted here is to model the antenna as a two-port network to find its equivalent ABCD parameters:

$$\begin{bmatrix} A_C & B_C \\ C_C & D_C \end{bmatrix} * \begin{bmatrix} A_C & B_C \\ C_C & D_C \end{bmatrix}^{-1} * \begin{bmatrix} A_L & B_L \\ C_L & D_L \end{bmatrix} * \begin{bmatrix} D_C & B_C \\ C_C & A_C \end{bmatrix} * \begin{bmatrix} D_C & B_C \\ C_C & A_C \end{bmatrix}^{-1} = \begin{bmatrix} A_L & B_L \\ C_L & D_L \end{bmatrix}. \quad (11)$$

TWO-PORT ANTENNA MODEL

The derivation of the two-port network for a single-port antenna system starts with presenting the antenna as a standard resonant RLC circuit (either a series or parallel, depending on the antenna type) consisting of a series resistance (R_a) and a reactance (X_a) [21], where R_a comprises a radiation resistance R_r and a loss resistance R_L. The relationship among these

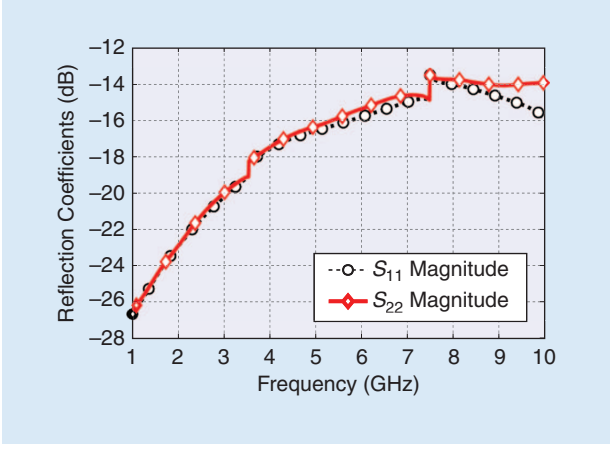

FIGURE 4. The connector reflection coefficients.

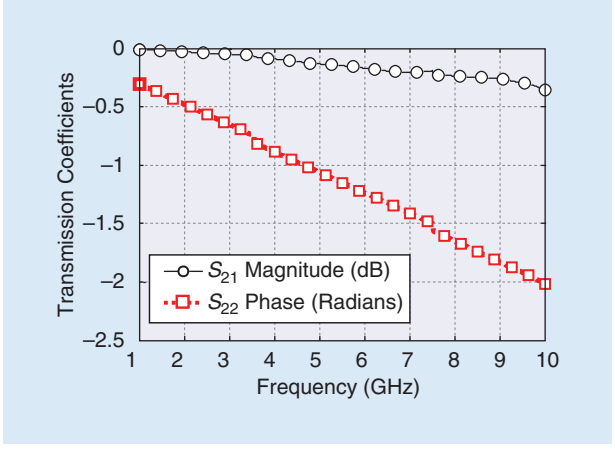

FIGURE 5. The connector transmission coefficients.

parameters is expressed in (12), where e is the antenna radiation efficiency and Z_a is the antenna impedance, which can be calculated from the measured antenna S-parameters according to (13), where Z_0 is the system characteristic (port) impedance (50-Ω). Since, R_r represents the energy radiated (delivered) in air, this can be replaced as the port 2 with a transformer to form a two-port equivalent antenna model as shown in Figure 7, where the transformer turn ratio N is defined as in (14) [22]:

$$Z_a = R_a + jX_a, \tag{12a}$$

$$R_a = R_r + R_L, \tag{12b}$$

$$R_L = (1-e)R_a, \tag{12c}$$

$$Z_a = Z_0 \frac{1+S_{11}}{1-S_{11}}, \tag{13}$$

and

$$N = \sqrt{\frac{R_r}{Z_0}}. \tag{14}$$

The two-port antenna model in Figure 7 is valid only for a single frequency point. However, this approach can be extended to a continuous two-port antenna model by calculating the overall ABCD parameters of the cascaded X_a, R_L, and the transformer at every frequency point. Thus, the ABCD parameters of the equivalent antenna model can be expressed in (15), where X_a, R_L, and N are calculated according to the relationships (12)–(14). The MATLAB program for this operation is shown in Figure 8. For simplicity, antenna radiation efficiency e is considered to be 1, and thus R_L is ignored since this is not going to affect the de-embedding performance. Then the equivalent two-port parameters of the measured patch antenna are calculated and illustrated in Figure 9 for the patch antenna shown in Figure 6. The equivalent two-port antenna model shows the preferred unaltered matching characteristics. Also, the antenna model shows symmetric antenna characteristics ($S_{11} = S_{22}$), and the transmission coefficient follows the relationship expressed in (16) where e is considered to be 1.

$$\begin{bmatrix} A & B \\ C & D \end{bmatrix}_{\text{Antenna}} = \begin{bmatrix} 1 & jX_a \\ 0 & 1 \end{bmatrix} * \begin{bmatrix} 1 & R_L \\ 0 & 1 \end{bmatrix} * \begin{bmatrix} N & 0 \\ 0 & 1/N \end{bmatrix}, \tag{15}$$

$$|S_{21}| = (1 - |S_{11}|^2)e. \tag{16}$$

CONNECTOR DE-EMBEDDING AND ANTENNA CHARACTERIZATION

After finding the two-port antenna ABCD parameters, the connector effects can be de-embedded by cascading the inverse connector ABCD

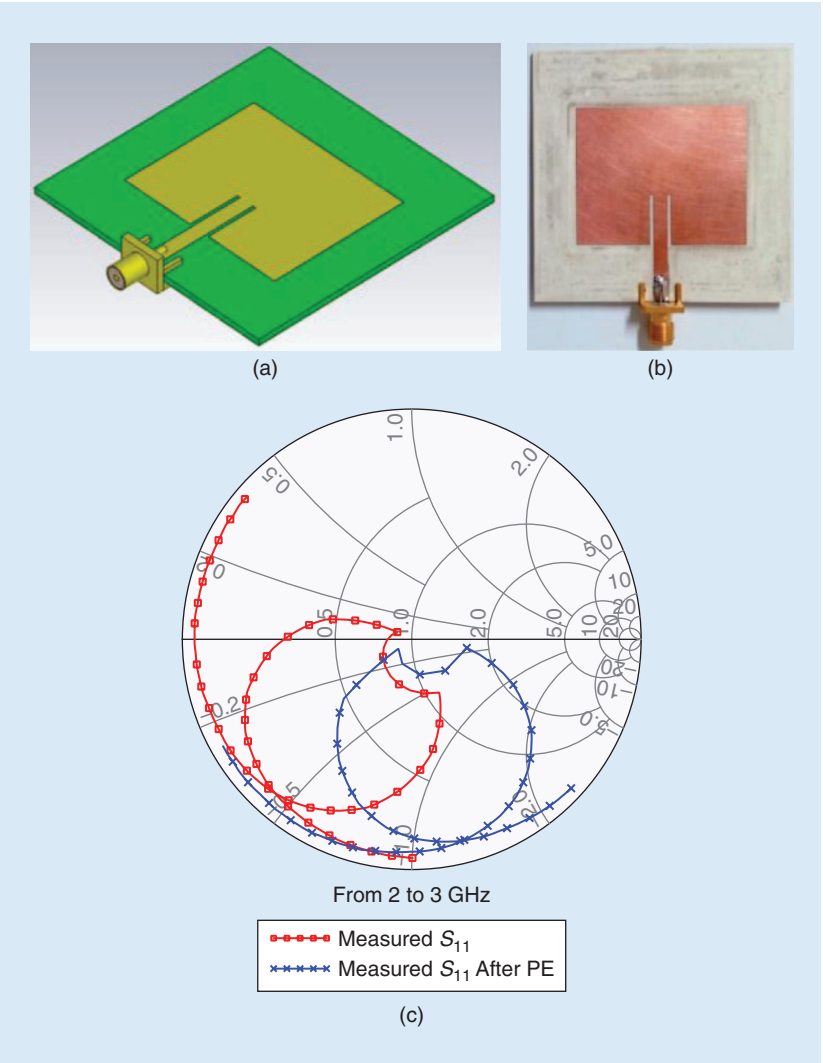

FIGURE 6. The patch antenna: (a) the model, (b) the prototype, and (c) the measured reflection coefficients before and after port extension.

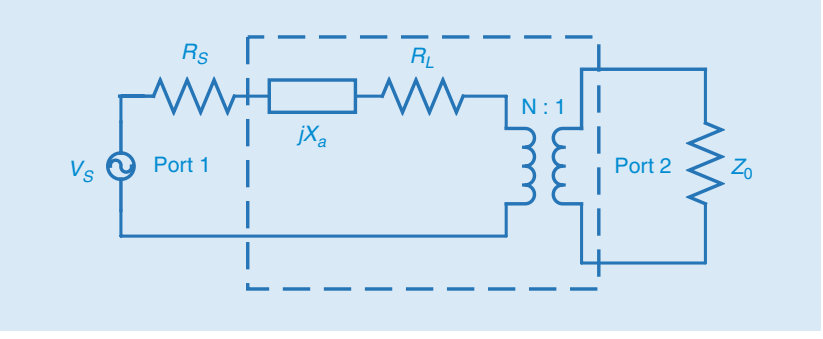

FIGURE 7. The two-port antenna equivalent network at a single frequency [22].

```
clear all; clc; close all;

%% Loading measured antenna S-parameter data
load antenna_meas_conn

s11a = real_s11+1i*imag_s11;

%% Calculating Antenna impedance from S-parameter
Za=50*(1+s11a)./(1-s11a);

%% Calculating Rr, Xa and N
Rr=real(Za);
Xa=imag(Za);
N=sqrt(Rr/50);

%% Finding equivalent antenna ABCD parameters

for k=1:length(freq)

    Xa_ABCD = [1 1i*Xa(k); 0 1];
    txf_ABCD = [N(k) 0; 0 1/N(k)];
    ant_ABCD = Xa_ABCD*txf_ABCD;
    ant_sparams = abcd2s(ant_ABCD,50);
    s11(k,1) = ant_sparams(1,1);
    s12(k,1) = ant_sparams(1,2);
    s21(k,1) = ant_sparams(2,1);
    s22(k,1) = ant_sparams(2,2);
end

ant_sparams_2p = [freq real(s11) imag(s11) real(s21)...
    imag(s21) real(s12) imag(s12) real(s22) imag(s22)];
save ant_sparams_2p ant_sparams_2p
```

FIGURE 8. The MATLAB program for calculating the equivalent two-port antenna ABCD parameters.

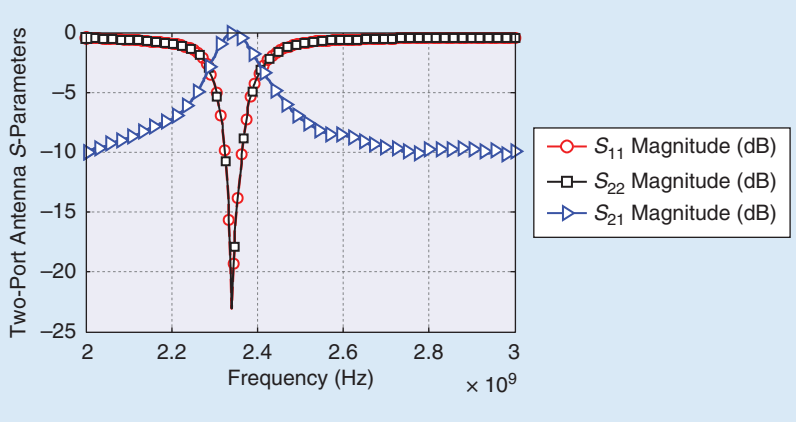

FIGURE 9. The equivalent two-port antenna S-parameters.

parameters, which is illustrated in Figure 10 and the results shown in Figure 11. The antenna reflection coefficient after the PE and the connector de-embedding are not the same in terms of the phase and magnitude as expected. Although the difference does not seem to be much, it can be significant in designing miniaturized active antenna systems, which are highly selective in nature and can be easily detuned by such inaccuracies, especially when including the component tolerances. This scenario is better observed by the application examples discussed in the next section.

The overall procedure of connector de-embedding and the single-port antenna characterization can be summarized as follows:

1) Measure two T-lines with different lengths and find the parameters J and K as shown in Figure 2(b).
2) Model the T-lines and find the parameters M and N as shown in Figure 2(a).
3) Find the connector parameters W, X, and Y from J, K, M, and N according to (3)–(10). Then find the Z-parameters of the connectors.
4) Measure the single-port antenna and deduce the two-port antenna model according to (15) and Figure 8.
5) De-embed the connector effect by cascading the inverse connector ABCD matrix with the two-port antenna model as shown in Figure 10.

ACTIVE ANTENNA APPLICATION EXAMPLES

To appreciate the connector de-embedding procedure described here, the amplifier integrated active antenna systems presented in [6] and [9] are revisited. In these two articles, narrowband and wideband miniaturized active antennas as well as ultrawideband multiple-input, multiple-output (MIMO) active antenna systems are reported.

In the miniaturized active antenna system, a new approach to antenna miniaturization, i.e., conjugate matching and codesigning of the antenna and amplifier, is investigated. Instead of designing the antenna and

amplifier separately, they are codesigned to achieve conjugate matching at the frequency of interest, which can provide antenna miniaturization and reduce the mismatch loss between the antenna and the amplifier. However, to achieve conjugate matching of an amplifier and a miniaturized antenna, both the phase and the magnitude of the antenna port parameters are important. The highly selective nature of miniaturized antennas also makes the accuracy requirement stringent. Thus, one of the necessary steps of such active antenna system design is the characterization of the antenna and the amplifier from the measurement results.

To investigate the effect of improper connector de-embedding, the patch antenna shown in Figure 6 is codesigned with an unmatched amplifier (mga-31689) and miniaturized from its original resonating frequency of 2.34–2.1 GHz by conjugate matching following the procedures presented in [6]. The antenna responses before and after connector de-embedding are shown in Figure 12. If the connector properties are not de-embedded, the antenna response is shifted from 2.1 to 1.8 GHz, with poor matching characteristics. If the connector de-embedding by the PE feature is considered, detuning still happens and the antenna response is shifted from 2.1 to 2.05 GHz, as mentioned in the section "Connector De-Embedding and Antenna Characterization." Although such a shift (50 MHz) does not seem to be much considering the narrow-band behavior (bandwidth of 25 MHz), the antenna is detuned from its desired operating band (narrow-band antennas are generally useful in band-selective applications where maintaining the desired operating band is crucial). Besides, such detuning is uncertain by nature; i.e., the shift in antenna response is not always going to be 50 MHz. Thus, the appropriate connector de-embedding and antenna characterization are vital in an active antenna design.

Similar results were reported in [6], where the narrow-band active antenna system was detuned from the desired 2.45 to 2.6 GHz, which was attributed to the modeling and de-embedding

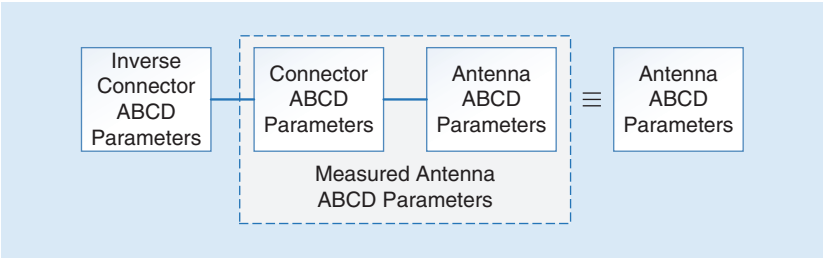

FIGURE 10. The de-embedding connector and the antenna characterization.

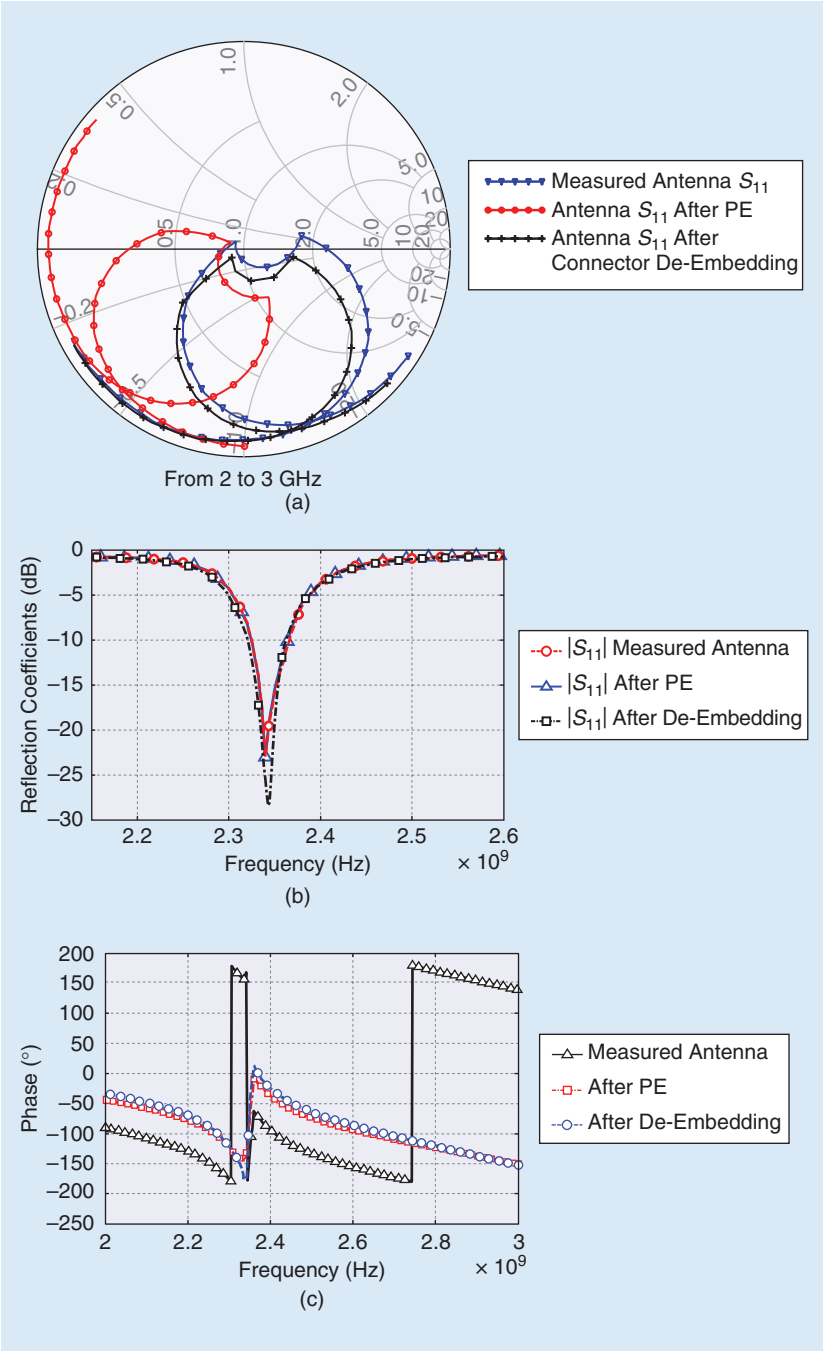

FIGURE 11. The de-embedded antenna S-parameters: (a) the complex S_{11}, (b) the magnitude of S_{11}, and (c) the phase of S_{11}.

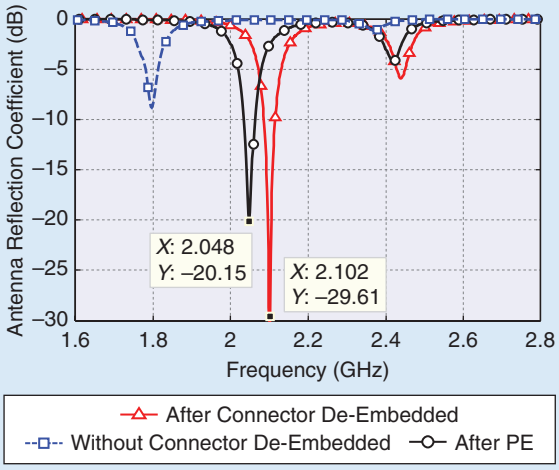

FIGURE 12. The active antenna reflection coefficients with connector de-embedding scenarios.

inaccuracy and component tolerances. Actually, the inaccurate calculation of the connector properties (phase and magnitude) misplaced the response on the Smith chart, making it hard to achieve conjugate matching at the desired frequency band and detuning consequently happening. However, following the appropriate de-embedding and modeling steps (including connectors as presented here), agreement between the measurement and target specifications (operating bandwidth of 2.45–2.6 GHz) for a wideband receiving active antenna had been reported [6]. The prototype and the antenna response are shown in Figure 13(a) and (b), respectively, with different

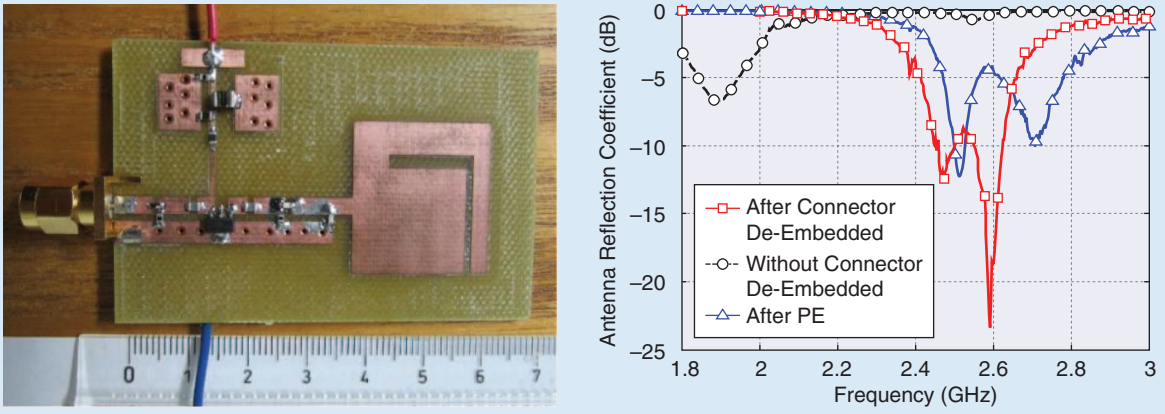

FIGURE 13. A miniaturized wideband active integrated antenna: (a) the prototype and (b) the reflection coefficients [6].

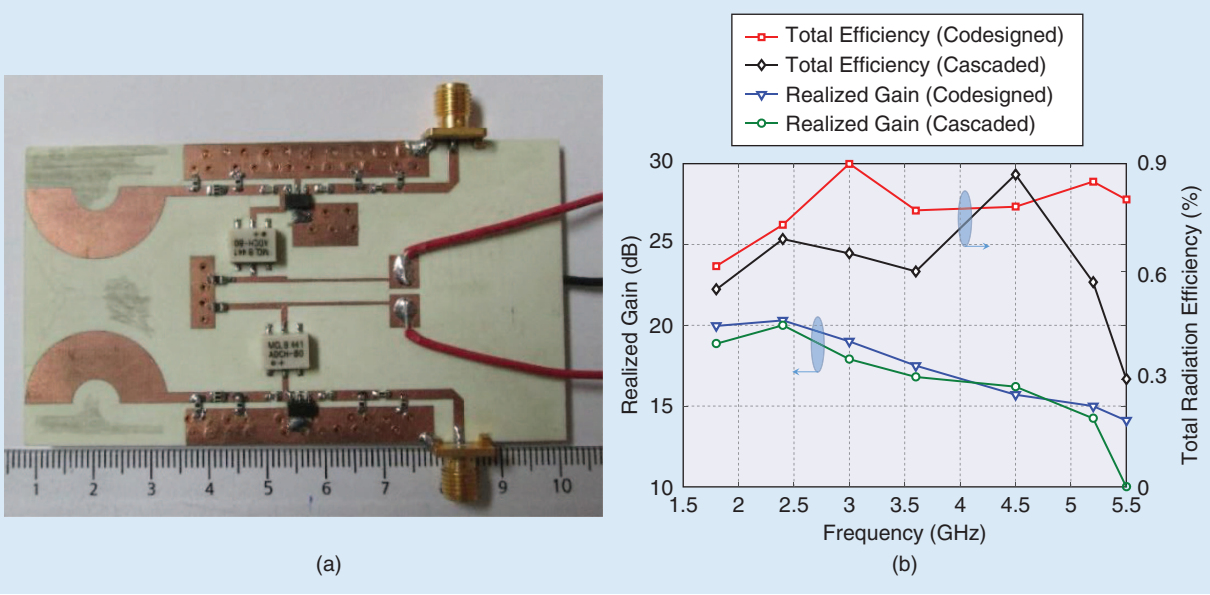

FIGURE 14. The MIMO active antenna system: (a) the prototype and (b) the radiation performance [7].

de-embedding scenarios. If the connector properties are not de-embedded properly during the antenna characterization, a shift in the operating frequency and a mismatch can happen, which eventually degrades the overall active antenna system performance.

For the active MIMO antenna system, improved system performance, such as total radiation efficiency and realized gain, is achieved by codesigning the antenna and amplifier for ultrawideband operation [9]. Such codesigning mainly reduces the mismatch loss between the antenna and the amplifier. Again, an accurate characterization of the antenna in terms of both the phase and magnitude response is required to design the output matching network of the amplifier precisely so that optimum performances are achieved. The prototype and the radiation performances are shown in Figure 14(a) and (b) for the active integrated MIMO antenna system presented in [9]. With proper modeling and codesigning, the radiation efficiency can be more than 60% over the band of 1.8–5.5 GHz, which can be dropped to 35% when cascading the amplifier and the antenna directly instead of codesigning. Again, an important step in the active integrated MIMO antenna design was the connector de-embedding from the measured antenna properties for accessing accurate antenna characteristics.

CONCLUSIONS

To characterize RF components from measurement results and access the unterminated measurement data, it is essential to de-embed the connector electrical properties. This article provides a detailed and step-by-step procedure of connector de-embedding from a single-port antenna system. For this purpose, a continuous two-port equivalent antenna network is derived from its measurement results and a complete procedure is presented for de-embedding the connector effects from a single-port system, i.e., antenna. The proper connector de-embedding step increases the accuracy of the active antenna system design and improves the overall system performance.

AUTHOR INFORMATION

Sagar K. Dhar (sagar.dhar@ucalgarly.ca) is working toward his Ph.D. degree in electrical and computer engineering at iRadio Lab, University of Calgary, Canada. His research interests include active and passive radio-frequency circuits and monolithic microwave integrated circuit design.

Mohammad S. Sharawi (msharawi@kfupm.edu.sa) is a professor of electrical engineering at King Fahd University of Petroleum and Minerals, Saudi Arabia. His research interests are multiple-input, multiple-output as well as active, reconfigurable, and millimeter-wave antenna systems.

Fadhel M. Ghannouchi (fghannou@ucalgary.ca) is a professor in the Department of Electrical and Computer Engineering, University of Calgary. He is a Tier l Canada Research Chair in intelligent radio-frequency radio technology and the director of the iRadio Lab, University of Calgary. His research interests include nonlinear modeling of microwave devices and systems and the design of power- and spectrum-efficient amplification systems for wireless and satellite communication.

REFERENCES

[1] Y. Y. Lin, C. H. Wu, and T. G. Ma, "Miniaturized self-oscillating annular ring active integrated antennas," *IEEE Trans. Antennas Propag.*, vol. 59, no. 10, pp. 3597–3606, Oct. 2011.

[2] Y. Y. Lin and T. G. Ma, "Frequency-reconfigurable self-oscillating active antenna with gap-loaded ring radiator," *IEEE Antennas Wireless Propag. Lett.*, vol. 12, pp. 337–340, Mar. 2013.

[3] C. H. Wu and T. G. Ma, "Self-oscillating semiring active integrated antenna with frequency reconfigurability and voltage-controllability," *IEEE Trans. Antennas Propag.*, vol. 61, no. 7, pp. 3880–3885, July 2013.

[4] A. Imtiaz, J. Lees, H. Choi, and L. T. Joshi, "An integrated continuous class-mode power amplifier design approach for microwave enhanced portable diagnostic applications," *IEEE Trans. Microw. Theory Technol.*, vol. 63, no. 10, pp. 3007–3015, Oct. 2015.

[5] H. Kim, I.-J. Yoon, and Y. J. Yoon, "A novel fully integrated transmitter front-end with high power-added efficiency," *IEEE Trans. Microw. Theory Techn.*, vol. 53, no. 10, pp. 3206–3214, Oct. 2005.

[6] M. S. Sharawi, S. K. Dhar, O. Hammi, and F. M. Ghannouchi, "Miniaturized active integrated antennas: A co-design approach," *IET Microw., Antennas Propag.*, vol. 10, no. 8, pp. 871–879, June 2016.

[7] S. K. Dhar, M. S. Sharawi, and F. M. Ghannouchi, "An electrically small wideband antenna with tunable non-foster matching network," in *Proc. 10th European Conf. Antennas and Propagation (EuCAP)*, 2016, pp. 1–4.

[8] H. Mirzaei and G. V. Eleftheriades, "A resonant printed monopole antenna with an embedded non-foster matching network," *IEEE Trans. Antennas Propag.*, vol. 61, no. 11, pp. 5363–5371, Nov. 2013.

[9] S. K. Dhar, M. S. Sharawi, O. Hammi, and F. M. Ghannouchi, "An active integrated ultra-wideband MIMO antenna," *IEEE Trans. Antennas Propag.*, vol. 64, no. 4, pp. 1573–1578, Apr. 2016.

[10] D. Weinstein, "How does one ensure high performance with minimal reflections and losses?," *Amphenol RF Connection Mag.*, vol. 2, no. 2, pp. 6–7, Oct. 2003.

[11] J. S. Wight, O. P. Jain, W. J. Chudobiak, and V. Makios, "Equivalent circuits of microstrip impedance discontinuities and launchers," *IEEE Trans. Microw. Theory Technol.*, vol. 22, no. 1, pp. 48–52, Jan. 1974.

[12] M. A. Goodberlet and J. B. Mead, "Microwave connector characterization," *IEEE Microw. Mag.*, vol. 7, no. 5, pp. 78–83, Oct. 2006.

[13] J. C. Rautio, "A de-embedding algorithm for electromagnetics," *Int. J. Microw. Mill.-Wave Comput.-Aided Eng.*, vol. 1, no. 3, pp. 282–287, Jan. 1991.

[14] R. F. Bauer and P. Penfield, "De-Embedding and unterminating," *IEEE Trans. Microw. Theory Technol.*, vol. 22, no. 3, pp. 282–288, Mar. 1974.

[15] N. Erickson, K. Shringarpure, J. Fan, B. Achkir, S. Pan, and C. Hwang, "De-embedding techniques for transmission lines: An exploration, review, and proposal," in *Proc. 2013 IEEE Int. Symp. Electromagnetic Compatibility (EMC)*, pp. 840–845.

[16] A. M. Mangan, S. P. Voinigescu, M.-T. Yang, and M. Tazlauanu, "De-embedding transmission line measurements for accurate modeling of IC designs," *IEEE Trans. Electron Devices*, vol. 53, no. 2, pp. 235–241, Feb. 2006.

[17] N. Li, K. Matsushita, N. Takayama, S. Ito, K. Okada, and A. Matsuzawa, "Evaluation of a multiline de-embedding technique up to 110 GHz for millimeter-wave CMOS circuit design," *IEICE Trans. Fundamentals Electron. Commun. Computer Sci.*, vol. E93–A, no. 2, pp. 431–439, Feb. 2010.

[18] V. Ricchiuti, A. Orlandi, and G. Antonini, "De-embedding methods for characterizing PCB interconnections," in *Proc. 9th IEEE Workshop Signal Propagation Interconnects*, 2005, pp. 65–68.

[19] D. Pinchera and M. D. Migliore, "A simple and effective procedure for connector de-embedding in antenna arrays," *IEEE Antennas Wireless Propag. Lett.*, vol. 8, pp. 534–537, Mar. 2009.

[20] D. Ballo. (1998). Applying error correction to network analyzer measurements. *Microwave Journal*. [Online]. Available: http://www.microwavejournal.com/articles/2277-applying-error-correction-to-network-analyzer-measurements

[21] C. A. Balanis, *Antenna Theory: Analysis and Design*, 3rd ed. Hoboken, NJ: Wiley-Interscience, 2005.

[22] J. T. Aberle, "Two-port representation of an antenna with application to non-foster matching networks," *IEEE Trans. Antennas Propag.*, vol. 56, no. 5, pp. 1218–1222, May 2008.